

Theme Article-3

**T.3: Total external reflection x-ray fluorescence spectrometry**

*M.K.Tiwari (mktiwari@cat.ernet.in) and G.S.Lodha*

X-ray fluorescence (XRF) spectrometry is a well-established technique for elemental analysis at micro and trace level. The detection of emitted characteristic fluorescence x-rays is normally carried out either by a wavelength dispersive technique or by energy dispersive technique. In the wavelength dispersive mode, a crystal monochromator is used for the dispersion of different characteristic x-rays. In the energy dispersive mode, usually a solid state x-ray detector (e.g. Si(Li) detector) is employed as an energy dispersive device. In the total external reflection x-ray fluorescence spectrometry (TXRF), the specimen is excited by the primary x-ray beam at a glancing angle less than the critical angle  $\phi_c$  (Fig.T.3.1a). The sample is excited by the x-ray standing wave field intensity generated on the flat surface due to interference of incident and reflected beam (Fig.T.3.1b). The penetration depth of the primary x-ray beam inside the sample surface is

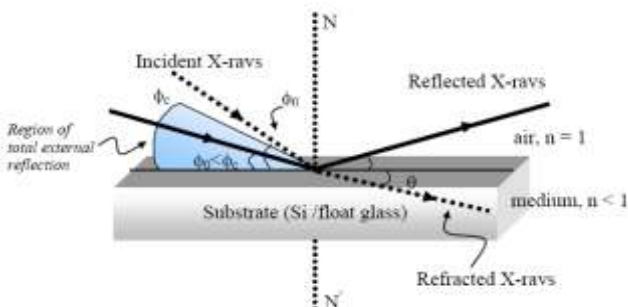


Fig. T.3.1a: Reflection and refraction of x-rays on flat surface.

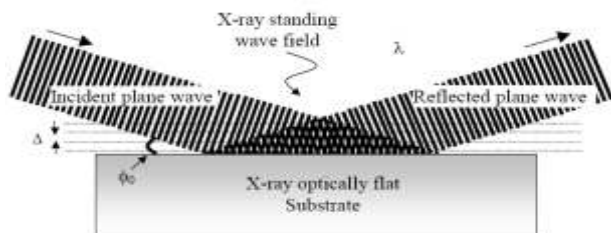


Fig. T.3.1b: The super position of two plane waves on a reflector surface under total external reflection condition. For incidence angles  $0 < \phi_0 < \phi_c$  a standing wave field of periodicity  $\lambda$  is generated on top of the surface.

restricted to a few nanometers. This allows the application of TXRF for ultra-trace elemental analysis. Due to low penetration depth of the primary x-ray beam, the primary

beam does not interact with the sample bulk. Thus, possibility of Compton scattering is drastically reduced resulting in improved sensitivities compared to conventional XRF. Keeping in view the applicability and several attractive merits of this technique, we (at Synchrotron Utilization and Materials Research Division) have designed and constructed a versatile TXRF spectrometer [1,2] and are using it for a variety of applications. The performance of the TXRF spectrometer and the various applications for which it has been used for, are briefly described.

For small values of the incidence angle  $\phi_0 (< \phi_c)$ , the phase shift between the incident and the reflected x-ray beam would be  $\sim 180^\circ$ . In this condition, the node of the x-ray standing wave field coincides with the surface of the substrate. At critical angle, the phase shift is close to zero and an anti node exists near the surface. Changing the incidence angle between near zero to critical angle can move the node - anti node distance and their positions with respect to the surface of the substrate. One can use this x-ray standing wave field as a probe to find out the location of an impurity atom near the surface. One observes the fluorescence intensity from an impurity atom excited by the x-ray standing wave (XSW) field as a monitor for the location. The fluorescence intensity will be larger when the position of an impurity atom coincides with the position of an anti node. A low fluorescence signal is observed if the node of the x-ray standing wave field coincides with the position of impurity atom. Beyond the critical angle, the reflected intensity becomes weak, thereby decreasing the contrast of the x-ray standing wave field on the flat surface and only a small modulation in the fluorescence intensity is observed. In this condition, the primary incident beam mainly performs fluorescence excitation.

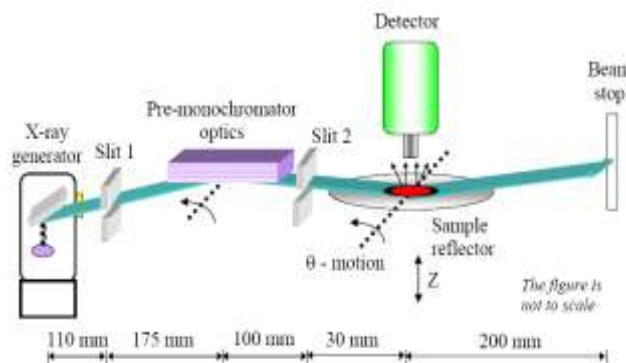


Fig. T.3.2a: A schematic arrangement of the TXRF set-up developed at RRCAT.

Figure T.3.2a shows a schematic ray diagram of this spectrometer while Fig. T.3.2b shows its photograph. Most of the components of this spectrometer have been designed and constructed in-house. It comprises of an x-ray generator, a slit-collimator arrangement, a monochromator stage (First reflector), a sample reflector stage (Second reflector), and an x-ray detection system. The system is set up on a 2 kW sealed x-ray tube with fine line focus. Before impinging x-ray beam on the sample reflector, it is important to monochromatize it using suitable monochromator (e.g. cutoff reflector, multilayer monochromator, etc.). As a monochromator, we have employed a Ni/C multilayer monochromator [ $d = 7.0$  nm,  $\theta = 0.47^\circ$ ,  $N = 30$ ] fabricated in our laboratory. It provides well-resolved Cu-K ( $8.05$  keV) radiation with a bandwidth of  $\sim 400$  eV for sample excitation. The detection system for energy dispersive measurement consists of a Peltier cooled solid-state detector, a spectroscopy amplifier and a multi channel pulse height analyzer installed in a personal computer. The solid state detector has an energy resolution of  $170$  eV at  $5.9$  keV and operates without liquid nitrogen. The detector was placed very close and normal to the sample substrate at a distance of  $\sim 4$  mm, so that a large solid angle is intercepted, which maximizes the counting efficiency. The provision has also been provided to mount a Si(Li) detector in place of the Peltier cooled detector for more demanding applications of high count rate with better energy resolution and better hard x-ray detection efficiency. The mechanical details of the spectrometer developed have been described elsewhere [3].

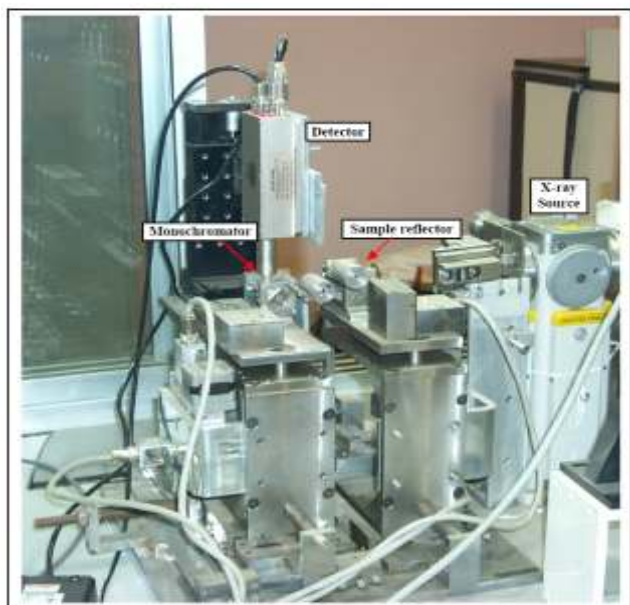


Fig.T.3.2b. TXRF spectrometer developed at RRCAT.

The effect of total external reflection of x-rays on the detection sensitivity has been demonstrated in Fig.T.3.3 wherein the fluorescence spectra recorded from a  $100$  ng aqueous residue of Fe, deposited on a float glass, are shown for two excitations geometries- normal excitation mode and total reflection mode. For the two modes, the angles are set to  $0.12^\circ$  and  $0.07^\circ$  that are respectively above and below the critical angle for float glass, which is  $\sim 0.1^\circ$  for Mo-K ( $17.444$  keV) x-rays. It can be seen from Fig. T.3.3a, in non-TXRF mode, a large Ca fluorescence signal from the glass material as well as large spectral background is observed because of deep penetration of primary beam into the substrate. On the other hand, in total reflection mode, as shown in Fig. T.3.3b, only the specimen residue deposited on the carrier surface gets excited. In TXRF mode, the primary beam does not penetrate into float glass substrate except a minimum penetration depth. This results a substantial reduction of Ca fluorescence intensity and the spectral background from the substrate. Moreover at the same time, the fluorescence intensity of analyte (Fe) increases due to two-fold excitation during incident and reflection beam path. As a result of these two conditions, one gets excellent elemental sensitivity in the TXRF mode. Fig.T.3.4, shows the elemental detection sensitivities of various elements achieved with this spectrometer. The detection limit values have been determined using Cu target x-ray tube with a tube power of  $40$  kV,  $25$  mA for an acquisition times of  $1000$  seconds. The detection sensitivities are in the range of  $2$ - $100$  pg for elements Ca to U at  $1$  kW x-ray tube power.

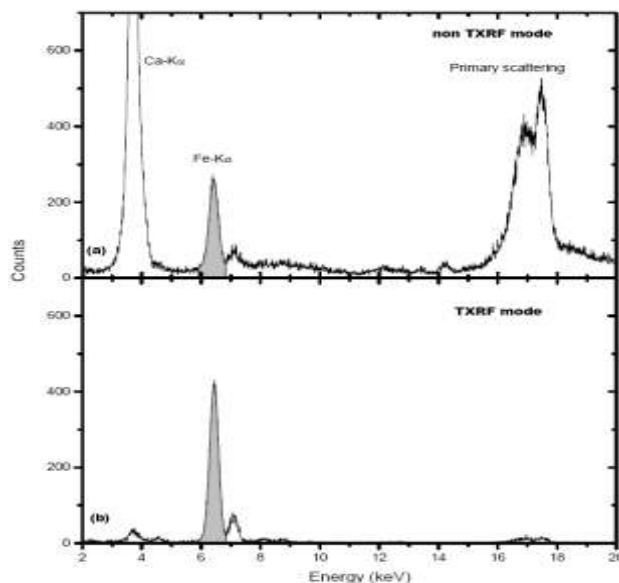


Fig. T.3.3: Fluorescence spectra recorded in two excitation geometries (Mo x-ray tube, 35kV, 10mA, 50s). (a) non TXRF mode: incidence angle set above the critical angle, (b) TXRF mode: incidence angle set below the critical angle

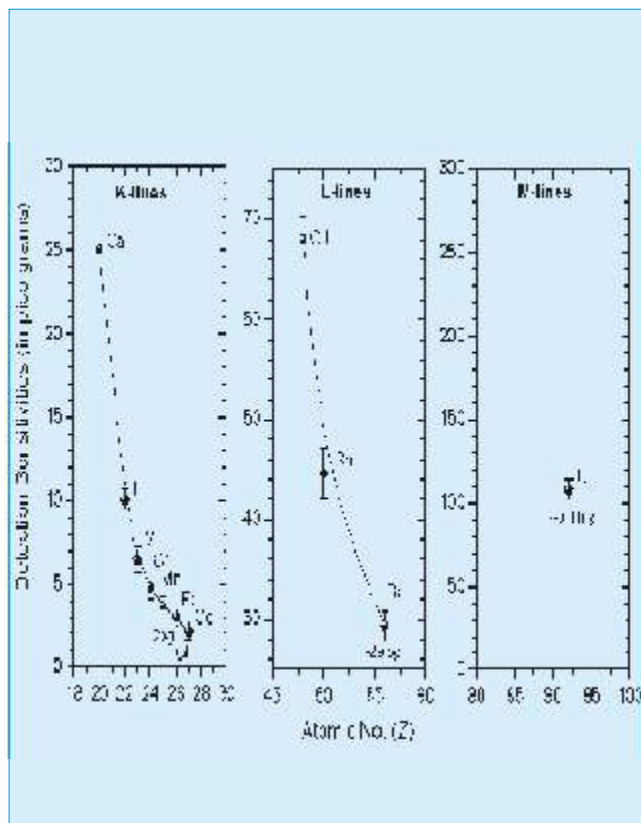


Fig.T.3.4: The detection limits determined by TXRF applied to residues of aqueous solutions at modest x-ray tube powers. Excitation source: Cu x-ray tube, 30 kV, 40 mA. Analysis time: 1000 s. Plots (a), (b) and (c), respectively show the DLs determined for K-series, L-series and M-series fluorescence lines.

In grazing incidence x-ray fluorescence (GIXRF) characterization, an angle dependent x-ray fluorescence profile needs to be recorded. Usually, in GIXRF analysis, the fluorescence measurements are carried out in the incidence angle range from  $0^\circ$  to  $2^\circ$  in a step of  $0.01^\circ$  or less. D. K. G. de Boer [4] have presented detailed theoretical treatment for the model calculation of GIXRF intensity from layered materials. It has been demonstrated that by changing the glancing incidence angle, the depth sensitivity in layered materials can be enlarged into nanometer region. We have used our TXRF spectrometer for a variety of applications including surface characterization, thin film analysis and x-ray standing wave measurements [5-12].

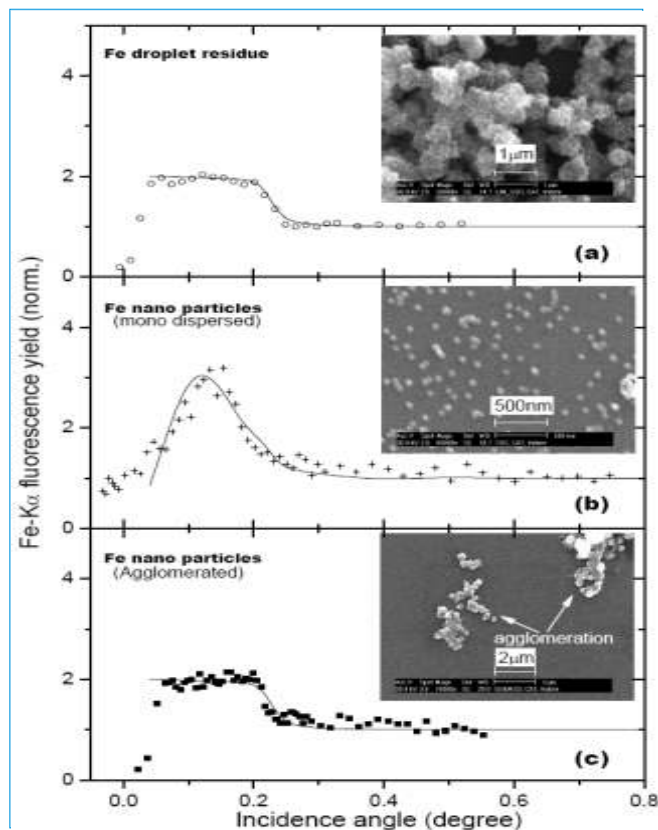


Fig.T.3.5: Recorded angle dependent x-ray fluorescence profiles for different forms of Fe particulate matter on top of a Si substrate. (a) droplet residue particles, (b) Fe nanoparticles (monodispersed), and (c) Fe nanoparticles (agglomerated). Scattered points show measured data whereas solid lines show fitted GIXRF profiles using CATGIXRF program. The insets show the SEM image of Fe particles in respective case.

Figure T.3.5 shows the recorded GIXRF profiles for Fe particles on top of a Si substrate in different situations [13]. Fig.T.3.5a shows a measured GIXRF profile for Fe droplet residue particles. Figs.T.3.5b and 5c show the measured GIXRF profiles in case of monodispersed nanoparticles and agglomerated nanoparticles respectively on a Si substrate. It can be seen that the XSW field generated on top of the substrate surface can be used to determine average vertical height of the nanoparticles. The best-fit GIXRF result determines average vertical heights of Fe nanoparticles  $\sim 19$  nm, which has been confirmed independently using atomic force microscopy (AFM) and scanning electron microscopy (SEM) techniques. The insets show the SEM pictures in respective case. In case of

agglomerations of particles (Fig.T.3.5c), the nanoparticles form micron size particles. The fluorescence profile becomes insensitive to the particle size distribution in this case and one obtains GIXRF profile as observed in case of Fe droplet residue particles. Thus, GIXRF profile is fairly sensitive to the mono dispersion of nanoparticles on the substrate surface.

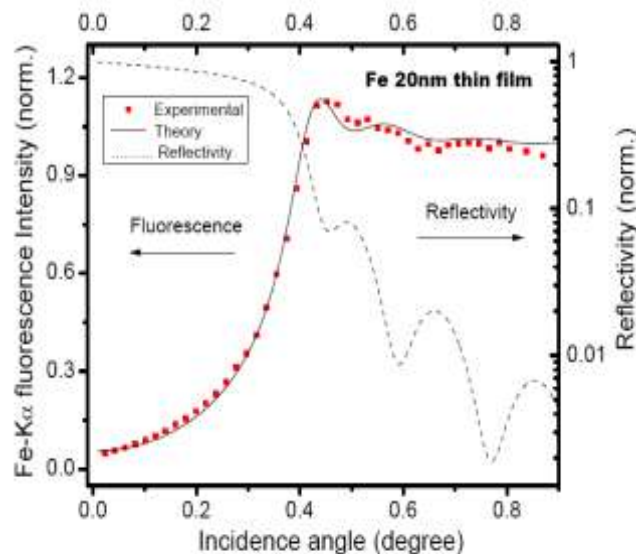


Fig.T.3.6: GIXRF profile of a 20 nm Fe thin film. Scattered points show the experimental data where as solid line shows fitted GIXRF profile. Dotted line shows calculated reflectivity for the same.

Using GIXRF measurement, one can estimate the thickness of a thin film structure. In Fig.T.3.6, we show the measured GIXRF profile for a 20 nm thick Fe thin film. In this figure, both GIXRF profile and calculated x-ray reflectivity has been plotted as a function of incidence angle. The figure shows that the fluorescence intensity and reflectivity are complimentary to each other, i.e. fluorescence is minimum at places where reflectivity is maximum and vice versa. The fluorescence intensity of Fe-K increases rapidly as incidence angle changes from 0 to critical angle of the layer medium. [ $\theta_c(\text{Fe}) = 0.384^\circ$  for 8.05 keV x-ray energy]. The fringe oscillation in GIXRF profile appears due to the interference of incoming and reflected beam. At higher incidence angles, the fluorescence intensity becomes nearly constant because the reflected part of the primary beam decreases abruptly and only incident beam excites the material. For the present case study, the best-fit result has been obtained for a film thickness of  $19.5 \pm 0.5\text{nm}$ , these values match reasonably well with the measurements

done independently using x-ray reflectivity method.

We have demonstrated x-ray standing wave characterization of a Ni/C periodic multilayer structure. In Fig.T.3.7, the normalized Ni-K fluorescence intensity has

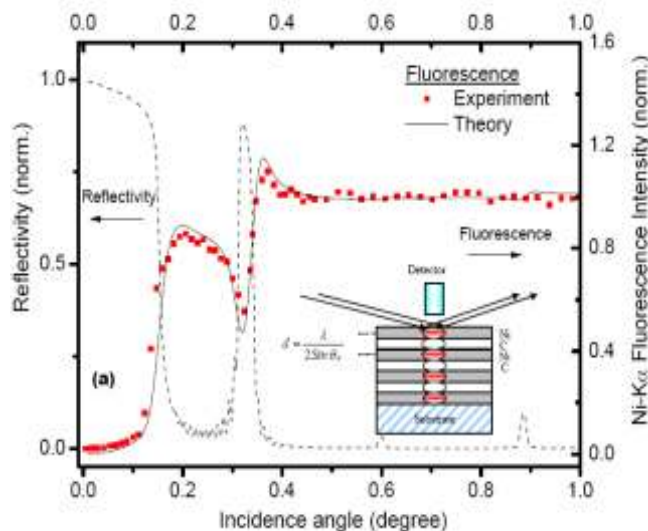


Fig.T.3.7: Measured GIXRF profile for Ni/C multilayer optics. Scattered point and solid line respectively show the experimental and fitted GIXRF profiles where as dotted line show the calculated reflectivity for the same.

been plotted along with the reflectivity profile as a function of the grazing incidence angle. One can see that in the vicinity of 1<sup>st</sup> Bragg peak, Ni-K fluorescence intensity is modulated in a special way. The XSW antinodes are in low-density layers (i.e. carbon layers) at low angle side of Bragg peak. As incidence angle changes across the Bragg position the standing wave antinodes move inward and finally coincide with high-density layers (Ni layers) at higher angle side of the Bragg peak. The measured XSW profile for a Ni/C multilayer [N = 20,  $\delta = 0.47$ , d = 7.0 nm] was found to match closely with calculated profiles as shown by solids line. The results of XSW characterization have been described elsewhere [9]. One unique feature of the XSW measurement is that it contains phase sensitive information that is not available using other surface characterization techniques like x-ray reflectivity, x-ray diffraction, etc. The advantage of XSW technique is that one can unambiguously determine the position of an impurity element whether it is in high-density layer or in low-density layer. The position of a

foreign impurity element inside a multilayer structure can be determined within nanometer accuracy and with sensitivity  $\sim 10^{10}$  to  $10^{11}$  atoms/cm<sup>2</sup>.

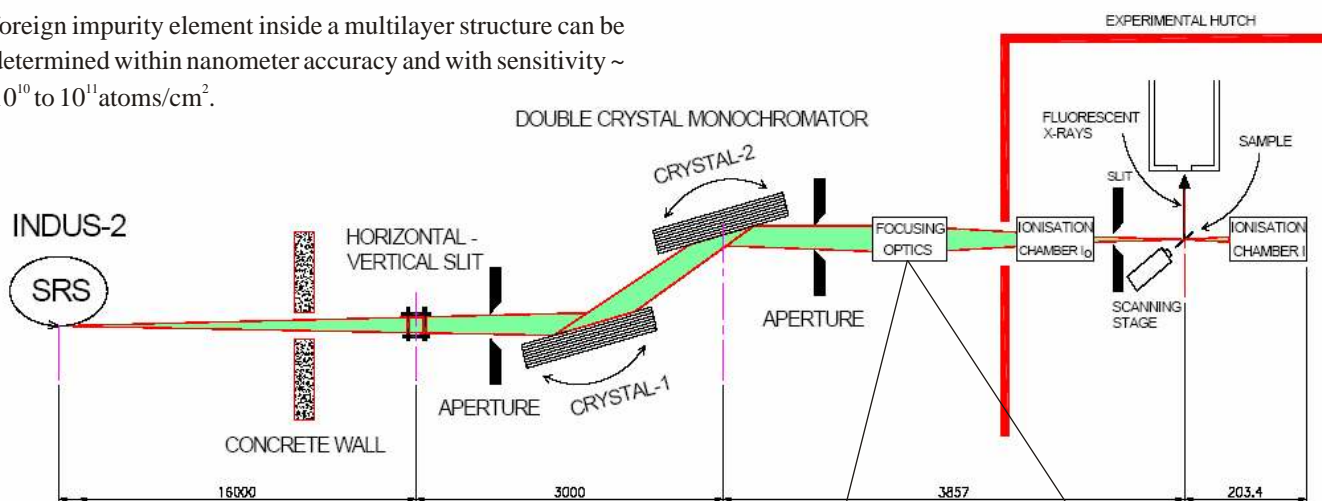
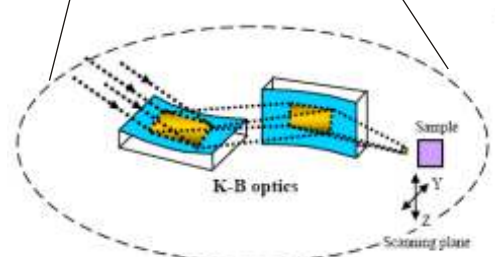


Fig. T.3.8: a) Optical layout of an x-ray fluorescence microprobe beam on Indus 2. b) Details of the focusing optics.

As an extension of the XRF activity, an x-ray fluorescence microprobe beam line has been designed and is under construction on Indus-2 synchrotron source. The optical layout of this beamline is shown in Fig.T.3.8. The microprobe XRF beamline will be installed on a bending magnet source ( $E_{crit} = 6.21$  keV). The beamline will work in the 3 – 20 keV photon range. It has been aimed to get a spatial resolution  $\sim 6\mu\text{m}$  (H)  $\times 12\mu\text{m}$  (V) at the sample position. The photon flux expected at the sample position is  $\sim 10^8$  photons/second. The maximum analysis area will be varied from few tens of microns to 25 mm. In this mode of analysis, it would be possible to perform nondestructive elemental mapping of samples. Apart from the elemental mapping, this beam line can also be used for other applications viz. TXRF analysis, normal XRF analysis, chemical speciation or near edge absorption spectroscopy, etc.



**References**

[1] M.K.Tiwari, B.Gowrishankar, V.K.Raghuvanshi, R.V. Nandedkar and K.J.S.Sawhney, Bull. Material Sci.25, 435 (2002).  
 [2] M.K.Tiwari, K.J.S.Sawhney, B.Gowrishankar, V.K. Raghuvanshi, and R.V.Nandedkar, Spectrochimica Acta Part B : Atomic Spectroscopy 59, 1141 (2004).  
 [3] M.K.Tiwari, in Ph.D. Thesis, Chapter 2, Devi Ahilya Vishwa Vidyalaya, Indore (2007).  
 [4] D.K.G. de Boer, Phys. Rev. B 44, 498 (1991).  
 [5] M.K.Tiwari, M.Nayak, G.S.Lodha and R.V. Nandedkar, Spectrochimica Acta Part B: Atomic Spectroscopy 62, 137 (2007).

[6] R.A.Ganeev, U.Chakravarty, P.A.Naik, H.Srivastava, M.K.Tiwari, and P.D. Gupta, Appl. Opt. 46, 1205, (07).  
 [7] A.Jaiswal, S.Rai, M.K.Tiwari, V.R.Reddy, G.S.Lodha and R.V. Nandedkar, J. Phys.: Condens. Matter 19, 016001 (2007).  
 [8] S.Rai, M.K.Tiwari, G.S.Lodha, M.H.Modi, M.K. Chattopadhyay, S.Majumdar, S.Gardelis, Z. Viskadourakis, J.Giapintzakis, R.V.Nandedkar, S.B.Roy, and P.Chaddah, Phys. Rev. B 73, 035417 (2006).  
 [9] M.K.Tiwari, S.R.Naik, G.S.Lodha, and R.V. Nandedkar, Analytical Sciences 21, 757 (2005).  
 [10] M.K.Tiwari, M.H.Modi, G.S.Lodha, A.K.Sinha, K.J.S.Sawhney, and R.V.Nandedkar, J. Non-Crystalline Solids 351, 2341 (2005).  
 [11] M.K.Tiwari, A.K.Singh, and K.J.S.Sawhney, Analytical Sciences 21, 143 (2005).  
 [12] M.K.Tiwari, and K.J.S.Sawhney, Spectrochimica Acta Part B : Atomic Spectroscopy 58, 1895 (2003).  
 [13] M.K.Tiwari, G.M.Bhalerao and A.K.Sinha, Submitted to Appl. Phys. Lett. (2007)